Supplementary Information

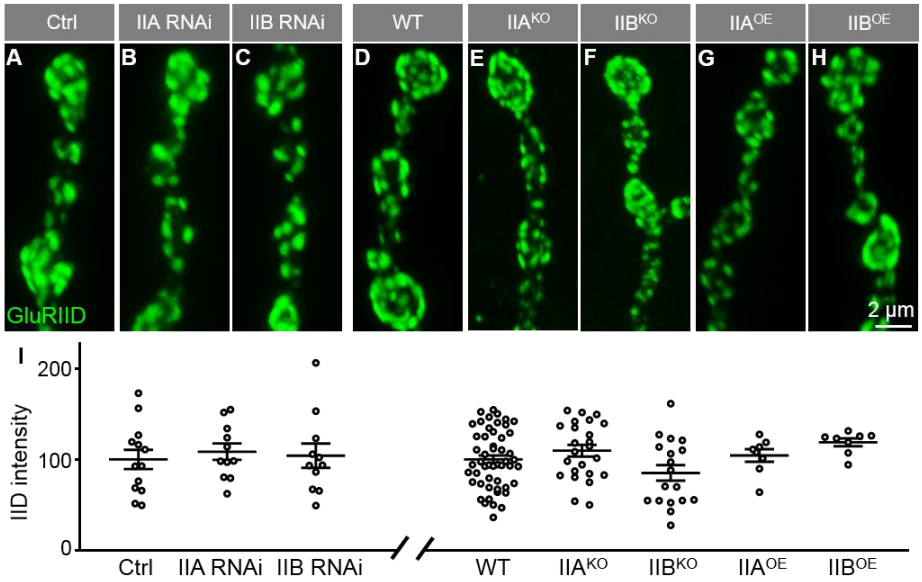

Fig. S1. Synaptic levels of GluRIID are normal when mutual negative regulation of GluRIIA and GluRIIB is induced. (A–H) Representative confocal images of third-instar larval NMJ4 stained with anti-GluRIID (green). The genotypes are Control (Ctrl: *C57-Gal4*, *UAS-Dicer2/+*), IIA RNAi (*C57-Gal4*, *UAS-Dicer2/UAS-GluRIIA-RNAi*), IIB RNAi (*C57-Gal4*, *UAS-Dicer2/UAS-GluRIIB-RNAi*), WT (w^{1118}), IIA^{KO} (*GluRIIA*^{SP16}), IIB^{KO}, IIA^{OE} (*Mhc-GluRIIA*), and IIB^{OE} (*Mhc-GluRIIB*). Scale bar: 2 µm. (I) Quantification of the fluorescence intensities of anti-GluRIID staining at the NMJ of different genotypes. Data are expressed as percentages of the Ctrl or WT fluorescence intensity. $n \geq 11$ NMJs for each genotype in A–C, $n \geq 18$ for each genotype in D–F, and $n = 8$ for each genotype in G and H. Error bars indicate s.e.m.

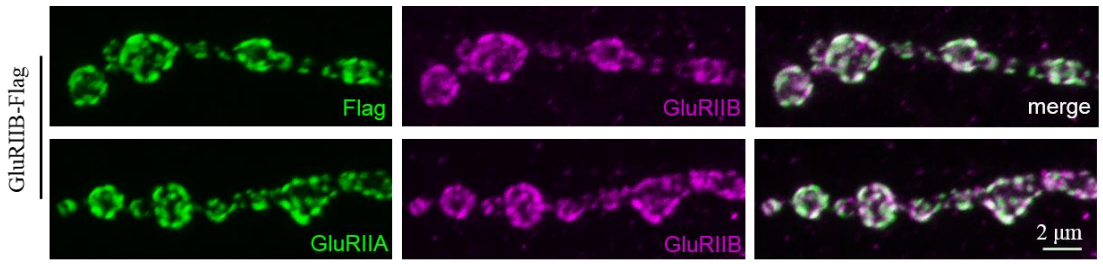

Fig. S2. Flag signals completely overlap with GluRIIB signals. Representative confocal images of third-instar larval NMJ4 co-stained with anti-GluRIIB (magenta) and anti-GluRIIA or anti-Flag (green). The genotype is homozygous *GluRIIB-Flag*. Scale bar: 2 μm.

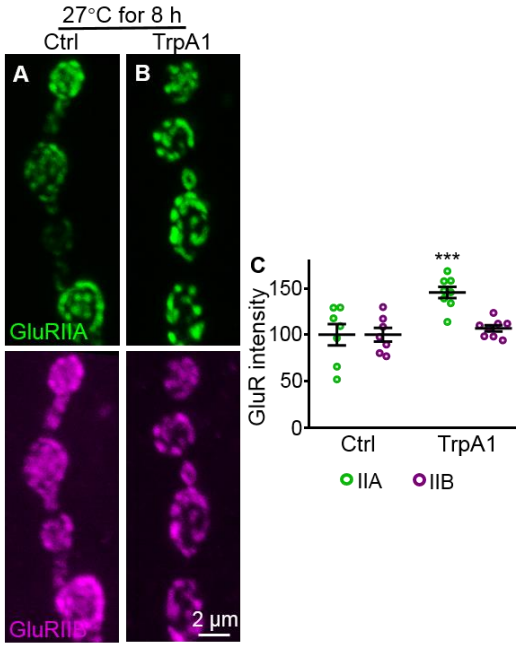

Fig. S3. Synaptic GluRIIA increases but GluRIIB remains unchanged when presynaptic neurotransmitter release is enhanced. (A,B) Representative confocal images of third-instar larval NMJ4 co-stained with anti-GluRIIA (green) and anti-GluRIIB (magenta). The genotypes are Control (A, *OK6-Gal4/+*) and TRPA1 (B, *OK6-Gal4/UAS-TRPA1*). Control and TRPA1 were intermittently stimulated by high temperature at 27°C for 8 h. Scale bar: 2 μm. (C) Quantification of the fluorescence intensities of anti-GluRIIA and anti-GluRIIB at the NMJ of different genotypes. $n \geq 7$. $^{***}p < 0.001$. Error bars indicate s.e.m.

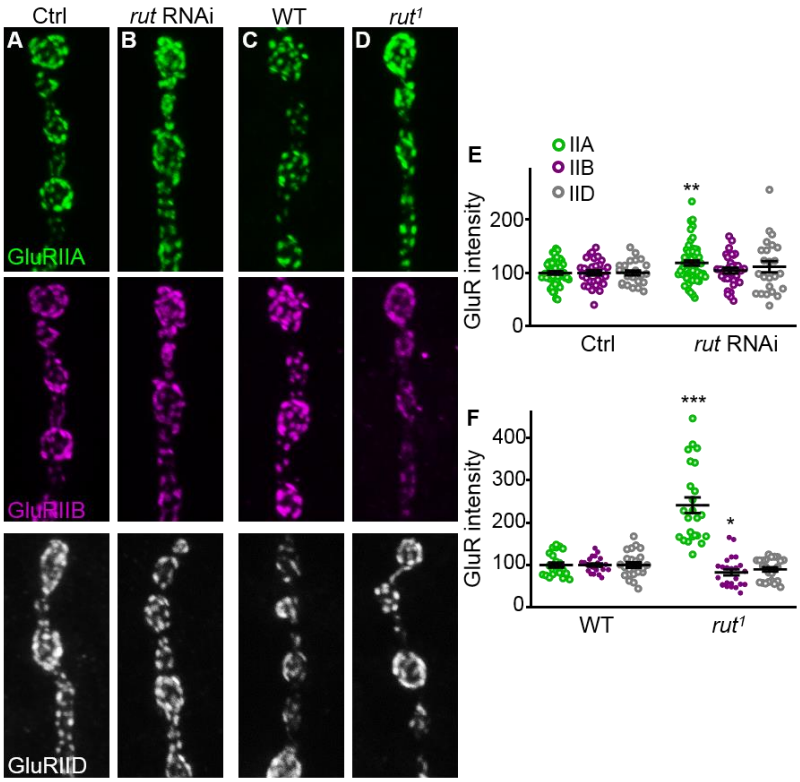

Fig. S4. cAMP downregulation results in increased GluRIIA but normal or reduced GluRIIB at NMJ synapses. (A–D) Representative images of NMJ4 synapses from different genotypes stained with anti-GluRIIA (green), anti-GluRIIB (magenta), and anti-GluRIID (gray). The genotypes are Control (Ctrl, *C57-Gal4/+*), *rut* RNAi (*UAS-rut-RNAi/+*; *C57-Gal4/+*), WT (w^{1118}) and rut^{1}. Scale bar: 2 μm. (E,F) Normalized intensities of the three GluR subunits at NMJ synapses from different genotypes. $n \geq 24$ for each genotypes. $^{*}p < 0.05$; $^{**}p < 0.01$; $^{***}p < 0.001$. Error bars indicate s.e.m.

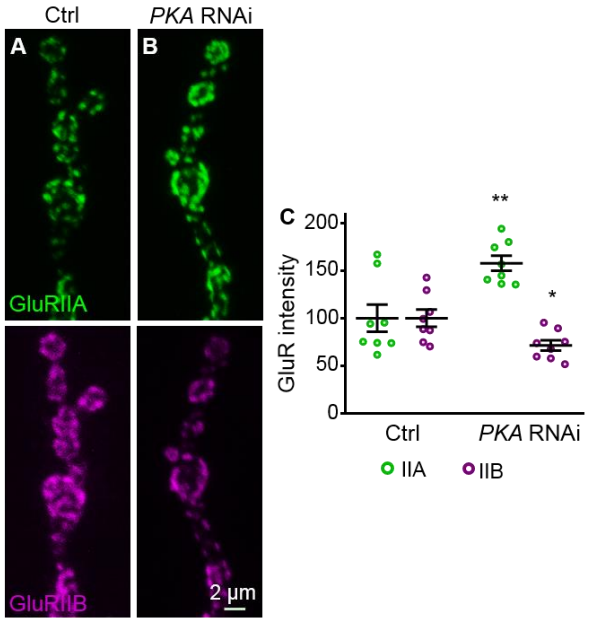

Fig. S5. Knockdown of *PKA-C1* in postsynaptic muscles leads to increased GluRIIA but reduced GluRIIB. (A,B) Representative images of NMJ4 synapses co-stained with anti-GluRIIA (green) and anti-GluRIIB (magenta). The genotypes are Control (Ctrl, *C57-Gal4/+*) and *PKA-C1* RNAi (*C57-Gal4/UAS-PKA-C1-RNAi*). Scale bar: 2 µm. (C) Normalized intensities of two GluR subunits at NMJ synapses. $n \geq 8$ for each genotypes. $^{*}p < 0.05$; $^{**}p < 0.01$. Error bars indicate s.e.m.

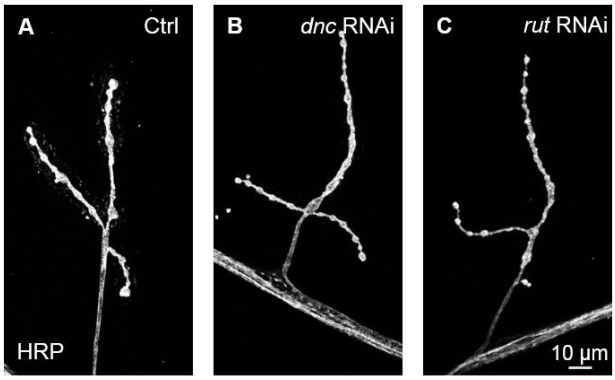

Fig. S6. The number of varicosities remains normal when *dnc* or *rut* is knocked down by RNAi in postsynaptic muscles. (A–C) Representative images of NMJ4 synapses stained with anti-HRP (gray). The genotypes are Control (Ctrl, *C57-Gal4/+*), *dnc* RNAi (*C57-Gal4/UAS-dnc* RNAi) and *rut* RNAi (*C57-Gal4/UAS-rut* RNAi). Scale bar: 10 µm.

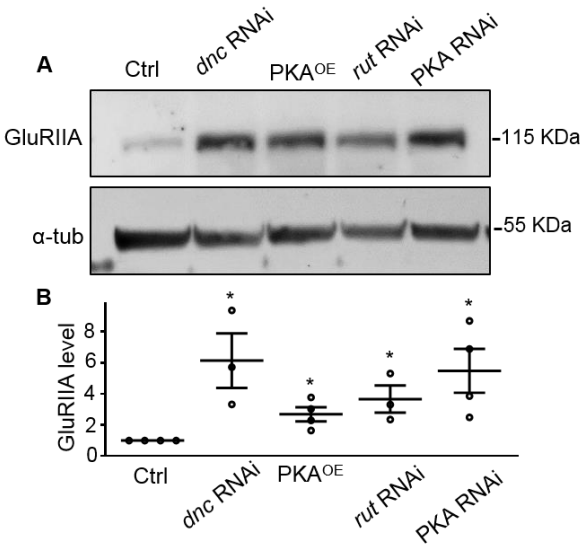

Fig. S7. The protein level of GluRIIA increases significantly when cAMP pathway is up- or down-regulated. (A) Representative western blots of muscle lysates probed with anti-GluRIIA. The full genotypes are as follows: Ctrl (*C57-Gal4/+*), *dnc* RNAi (*C57-Gal4/UAS-dnc RNAi*), PKA^{OE} (*C57-Gal4/UAS-PKA^{OE}*), *rut* RNAi (*UAS-rut-RNAi/+*; *C57-Gal4/+*), and *PKA-C1* RNAi (*C57-Gal4/UAS-PKA-C1-RNAi*). α-tubulin was used as a loading control. (B) Quantification of GluRIIA protein levels normalized to the α-tubulin control in different genotypes. $n \geq 3$. $^{*}p < 0.05$. Error bars indicate s.e.m.

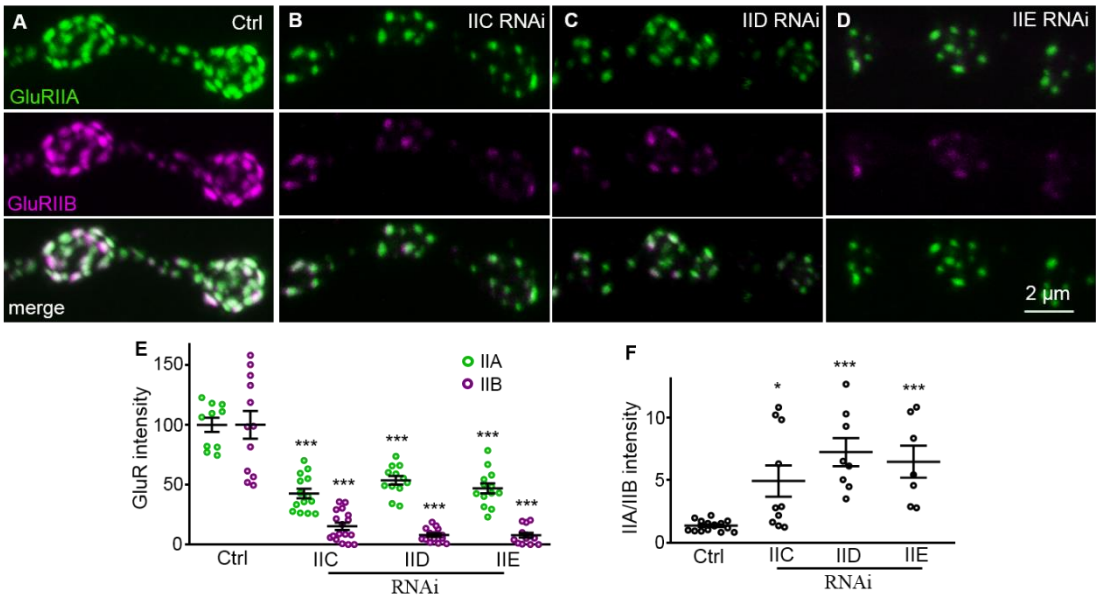

Fig. S8. Synaptic GluRIIA and GluRIIB decrease with the balance shifting towards more GluRIIA when an essential subunit of GluRs is knocked down. (A–D) Representative confocal images of late third-instar larval NMJ4 stained with anti-GluRIIA (green) and anti-GluRIIB (magenta). Full genotypes are as follows: Ctrl (*C57-Gal4/+*), IIC RNAi (*C57-Gal4/UAS-IIC RNAi*), IID RNAi (*C57-Gal4/UAS-IID RNAi*), and IIE RNAi (*C57-Gal4/UAS-IIE RNAi*). Scale bar: 2 µm. (E) Quantification of the intensities of anti-GluRIIA and anti-GluRIIB staining at the NMJ. Data are expressed as normalized staining intensities with respect to Ctrl. $n \geq 10$ for each genotype. (F) Quantification of the ratio of GluRIIA to GluRIIB intensities. $^{*}p < 0.05$; $^{***}p < 0.001$. Error bars indicate s.e.m.

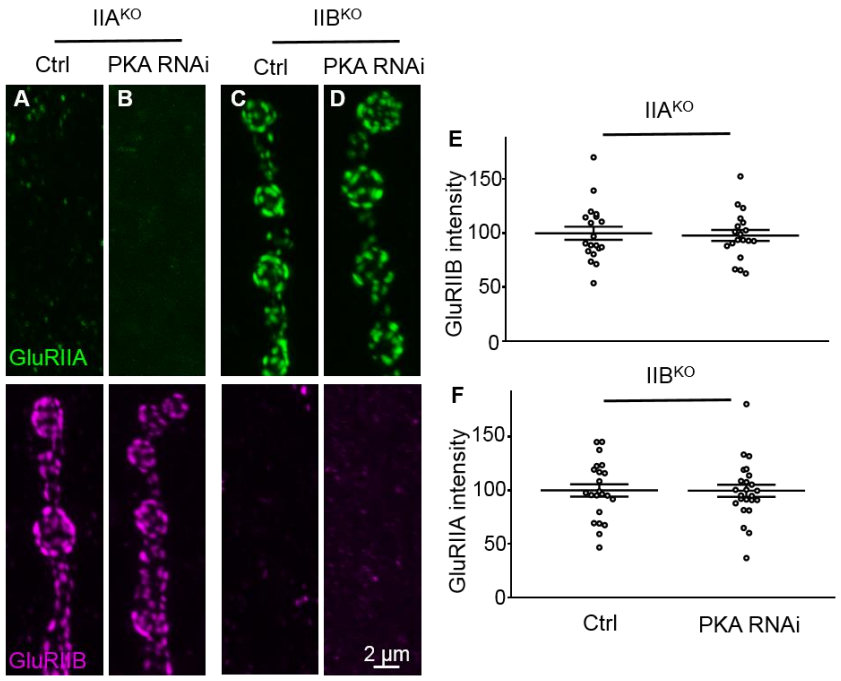

Fig. S9. The antagonistic balance of GluRIIA/GluRIIB does not require the cAMP pathway on the postsynaptic side. (A–D) Representative images of NMJ4 synapses from different genotypes stained with anti-GluRIIA (green) and anti-GluRIIB (magenta): IIA^{KO} Ctrl (*IIA^{SP16}; C57-Gal4/+*, A), IIA^{KO} PKA RNAi (*IIA^{SP16}; C57-Gal4/UAS-PKA RNAi*, B), IIB^{KO} Ctrl (*IIB^{KO}; C57-Gal4/+*, C), and IIB^{KO} PKA RNAi (*IIB^{KO}; C57-Gal4/UAS-PKA RNAi*, D). Scale bar: 2 µm. (E,F) Normalized intensities of GluRIIB and GluRIIA at NMJ synapses from different genotypes. $n \geq 19$ for each genotype. Error bars indicate s.e.m.

Table S1. Genes that do not affect synaptic expression of GluRIIA and GluRIIB when knocked down by *C57-Gal4*-driven RNAi in postsynaptic muscles

Click here to Download Table S1